2. Basic Principles

2.1 Theoretical aspects

This section presents some basic theoretical aspects of NMR which are relevant for a technical discussion of the principles and experimental procedures used when studying biological macromolecules in solution by NMR. A rigorous discussion of the theoretical foundation of NMR can be found in many textbooks [*e.g.* 16, 19, 24, 26, 29]. Only a very limited theoretical foundation is necessary for the technically oriented discussion of NMR methods in the following sections. The concept of energy levels, the Bloch equations and the product operator formalism are sufficient in most cases. NMR is intimately related with frequencies and to obtain a clear distinction between angular frequencies with units rad/s and technical frequencies in Hertz (Hz) the symbols ω or Ω are used for the former and ν for the latter.

The basis of all NMR experiments is the nuclear spin which can be interpreted as a magnetic moment. A spin $\frac{1}{2}$ nucleus in this view forms a small dipole. This dipole orients either parallel (α state) or antiparallel (β state) to a magnetic field leading to a small energy difference ΔE between the two states

$$\Delta E = \frac{h\gamma}{2\pi} B_o = \hbar \gamma B_o \qquad (2.1)$$

where B_o is a large externally applied homogeneous magnetic field, h is Planck's constant ($\hbar = h/(2\pi)$), and γ the gyromagnetic ratio which is a property of the nucleus and can have a

Table 1
Properties of selected nuclei

Nucleus	Spin	γ † [10^7rad/(Ts)]	natural abundance [%]	relative sensitivity§
^{1}H	$\frac{1}{2}$	26.75196	99.985	1.00
^{2}H	1	4.106625	0.015	$9.65\ 10^{-3}$
^{3}H	$\frac{1}{2}$	28.53495	-	1.21
^{13}C	$\frac{1}{2}$	6.72828	1.108	$1.59{\cdot}10^{-2}$
^{14}N	1	1.93378	99.634	$1.01{\cdot}10^{-3}$
^{15}N	$\frac{1}{2}$	–2.71262	0.366	$1.04{\cdot}10^{-3}$
^{17}O	$\frac{5}{2}$	–3.6281	0.037	$2.92{\cdot}10^{-2}$
^{19}F	$\frac{1}{2}$	25.18147	100.00	0.83
^{31}P	$\frac{1}{2}$	10.8394	100.00	$6.64{\cdot}10^{-2}$

† γ: gyromagnetic ratio; $\gamma\!\!\!^{-} = \gamma/(2\pi)$

§ For an equal number of nuclei relative to protons

positive or a negative value. Table 1 lists the gyromagnetic ratio and some other properties of nuclei important in NMR of biological macromolecules. From the two states of a dipole the α state is energetically slightly more favourable and thus possesses a higher population than the β state. Transitions between adjacent energy levels can be induced by small additional magnetic fields perpendicular to B_o which oscillate with a frequency ν_o fulfilling the resonance condition $\nu_o = \Delta E/h$. The frequency ν_o typically lies in the radio-frequency range and is often referred to as Larmor frequency. In the equilibrium state the Boltzmann distribution favours the lower energy states. Thus, the sum of all contributing nuclear magnetic moments of the individual nuclei leads to a resulting macroscopic magnetization M along the homogeneous external field B_o. In the framework of classical physics the behaviour of this magnetization under the action of time dependent magnetic fields can be described by the Bloch equations [30]. Because the spin is a quantum mechanical phenomenon this description has a very limited scope, but it proves very useful for the description of single resonance lines under the action of radio-frequency (*rf*) pulses and thus for the characterization of the effect of *rf* pulses.

2.1.1 Magnetization, precession and Bloch equations

In a classical description the macroscopic magnetization M created by the spins is described by a vector $\underline{M}$ parallel to the magnetic field vector $\underline{B}_o$. $\underline{M}$ is forced to move away from the direction of $\underline{B}_o$ by an additional linearly polarized magnetic field $\underline{B}_1$ perpendicular to $\underline{B}_o$. $\underline{B}_1$ must fulfil the resonance condition and oscillate with the resonance frequency ν_o. The magnetization vector $\underline{M}$ precesses about the resulting magnetic field $\underline{B} = \underline{B}_o + \underline{B}$ with an angular velocity vector $\underline{\omega}$ pointing in the opposite direction and the components as described in Eq. (2.2)

$$\underline{\omega} = -\gamma\underline{B} = -\gamma(2B_x \cos(2\pi\nu_o t + \phi), 2B_y \sin(2\pi\nu_o t + \phi), B_o) \tag{2.2}$$

where $\underline{\omega} = (\omega_x, \omega_y, \omega_o)$, $\underline{B}_o$ is chosen along the z axis and ϕ describes the angle between the x axis and $\underline{B}_1$. The magnetic field $\underline{B}_1$ is often applied only for short time periods as radio-frequency (*rf*) pulses. The discussion of the motion of the magnetization vector $\underline{M}$ in space due to *rf* pulses is usually based on a rotating frame of reference which has the same z axis along the static magnetic field $\underline{B}_o$ as the laboratory frame but rotates around the z axis with a frequency which is often chosen equal to the resonance frequency ν_o. In this rotating frame of reference the relevant component of the applied oscillating field $\underline{B}_1$ appears static making the discussion and visualization much easier. To fulfil the physical requirement that the magnetization vector $\underline{M}$ returns to its equilibrium position in a finite period of time after a disturbance, a longitudinal relaxation time T_1 (spin-lattice relaxation) is introduced. The loss of coherent precession is described by a transverse relaxation time T_2 (spin-spin relaxation). The motion of the magnetization vector $\underline{M}$ under the action of the magnetic field $\underline{B}$ and hence under $\underline{\omega}$ can be described by the Bloch equations [30]. These equations are presented in the Appendix for further reference.

In the rotating frame where $\underline{B}_1$ becomes static the main magnetic field $\underline{B}_o$ vanishes for nuclei with resonance frequency ν_o. Hence, Eq. (2.2) in this rotating frame contains only a transverse component $\underline{\omega} = -\gamma(B_1, 0, 0)$ with $\underline{B}_1$ chosen along the x axis. Consequently $\underline{M}$ precesses by an angle β around the magnetic field $\underline{B}_1$ applied as a pulse for the short duration τ

$$\beta = -\gamma B_1 \tau \tag{2.3}$$

where β is called the flip angle of the pulse. The flip angle is often indicated in degrees, for exam-

ple during a 90^o pulse $\underline{M}$ can precess from the *z* axis to the *x* axis. The angle β depends on γ and is negative for positive γ values such as for protons (Table 1). For positive γ values a magnetic field $\underline{B}_1$ pointing along the positive *x* axis turns $\underline{M}$ towards the negative *y* axis. A $\underline{B}_1$ field along the +y axis turns $\underline{M}$ towards the +*x* axis [16, 31]. When applying a *rf* pulse with a frequency differing from ν_o the action of the *rf* pulse becomes more complex as described in the Appendix. A situation often referred to as non-ideal behaviour of the *rf* pulses or as off-resonance effects.

The oscillating magnetic field $2B_1 \cos(\omega_{rf}t)$ used for excitation is linearly polarized in the laboratory frame. The transformation into the rotating frame can best be followed when this is thought of as a superposition of two counter-rotating, circular polarized fields with an amplitude B_1. When transforming into the rotating frame one component matches the Larmor frequency whereas the other oscillates at twice the Larmor frequency and does not fulfil the resonance condition. Bloch and Siegert [32] calculated the effect of the non-resonant field and found that it slightly shifts the frequency of the observed resonance lines away from the disturbing field by the small amount $\nu_B = (\gamma B_1)^2/\Delta\nu$ where $\gamma = \gamma/(2\pi)$ and $\Delta\nu$ stands for twice the resonance frequency. The Bloch-Siegert shift is small and amounts for example to 0.5 Hz for a frequency of 600 MHz during a *rf* pulse with duration τ of 10 μs and a flip angle of $\frac{\pi}{2}$ (Eq. (2.3) or 90^o. The shift disappears as soon as B_1 is switch off. An effect similar to the Bloch-Siegert shift occurs whenever a *rf* field is applied with a frequency $\Delta\nu$ off-resonance for the nuclear spins. First described by Ramsey [33] it is still very often referred to as Bloch-Siegert effect. To better distinguish it from the effect due to the counter rotating field the term "non-resonant effect" was introduced [34]. Since this additional field may be rather strong and close to the resonance frequency this effect can become quite large and should be compensated by adequate means [35] (Section 2.2.1).

2.1.2 Operators, coherence, and product operator formalism

The description of NMR experiments by the Bloch equations and by magnetization vectors in the rotating frame has rather significant limitations particularly for the description of multipulse experiments. On the other hand, a full quantum mechanical treatment which describes the state of the system by calculation of the time evolution of the density operator under the action of the appropriate Hamiltonian can be rather cumbersome. In a quantum mechanical description a *rf* pulse applied to the equilibrium state creates a coherent superposition of eigenstates which differ in their magnetic quantum number by one, often simply referred to as a coherence. In more complex experiments the magnetic quantum numbers between states may differ by a value *q* different from one, leading to a *q* quantum coherence with at least *q* spins involved. However only in-phase single quantum coherences (Table 2) are observable and correspond to the classical magnetization detected during the acquisition of an NMR experiment. Multiple quantum coherences cannot directly be observed but they influence the spin state and this information can be transferred to observable magnetization.

In a step towards a full quantum mechanical treatment the product operator formalism for spin $\frac{1}{2}$ nuclei was introduced [28]. In this approach it is assumed that there is no relaxation and that the difference in the resonance frequency $\Delta\nu$ of two nuclei is much larger than their mutual scalar coupling *J*; this situation is often referred to as weak spin-spin coupling whereas strong spin-spin coupling specifies the case where $\Delta\nu$ is close to or even smaller than *J*. With these assumptions simple rules can be calculated which describe the evolution of spin operators under the action of chemical shift, *J* coupling and *rf* pulses. The formalism combines the exact quantum mechanical treatment with an illustrative classical interpretation and is the basis for the development of many

NMR experiments. However, some parts of experimental schemes, for example TOCSY sequences (Section 4.2.1), can only be described with a full quantum mechanical treatment. Calculations with the formalism are not difficult, but many terms may have to be treated and implementations of the formalism within computer programs are very helpful in such situations [36, 37]. Although most of the experiments applied in biomolecular NMR correlate three or more spins, the majority of interactions can still be understood based on an analysis of two spins. For two spins I and S the operator basis for the formalism contains 16 elements. Two sets of basis operator, cartesian and shift operators, have proven very useful for the description of experimental schemes and are used in parallel. The two basis sets and the nomenclature used to characterize individual states are summarized in Table 2 [28].

Table 2
Product operator basis for a two spin system

cartesian operator basis	nomenclature	shift operator basis
I_z , S_z	longitudinal magnetization	I_z , S_z
I_x , I_y , S_x , S_y	in-phase transverse magnetization	I^+, I^-, S^+, S^-
$2I_xS_z$, $2I_yS_z$	anti-phase I spin magnetization	$2I^+S_z$, $2I^-S_z$
$2S_xI_z$, $2S_yI_z$	anti-phase S spin magnetization	$2S^+I_z$, $2S^-I_z$
$2I_xS_x$, $2I_yS_x$, $2I_xS_y$, $2I_yS_y$	two spin coherence	$2I^+S^+$, $2I^+S^-$, $2I^-S^+$, $2I^-S^-$
$2I_zS_z$	longitudinal two spin order	$2I_zS_z$
E	unity operator	E

The operators I_z and S_z are identical in the two basis sets and a simple relationship exists between the two other cartesian and shift operators:

$$\begin{aligned} I_x &= (I^+ + I^-)/2 & \qquad I^+ &= I_x + iI_y \\ I_y &= -i(I^+ - I^-)/2 & \qquad I^- &= I_x - iI_y \end{aligned} \tag{2.4}$$

Three operators, which represent the action of the Hamiltonians for chemical shift, scalar coupling and *rf* pulse, act on these basis operators and may transform them into other operators within the basis set. In this way the spin states created during a NMR experiment can be described and the observable magnetization calculated. The operator formalism can be summarized by simple rules [28] which are listed for both basis systems in the Appendix for further reference. Operators transform individually under these rules even in products of operators except for anti-phase terms which have to be considered as a unit and transformed accordingly, however, they can be treated consecutively when different couplings to the same nucleus exist.

The cartesian operators transform more easily under pulses and their single operators have a direct classical interpretation as magnetization vectors. The shift basis provides a useful alternative for the description of the evolution due to chemical shift and/or the influence of magnetic field gradients (Section 2.3) and is better suited for the description of coherence orders and coherence pathways (Fig. 1). Their single operators describe a transition from the α to the β state, I^+,

or from the β to the α state, I^-. Hence shift product operators are uniquely associated with one coherence order, for example I^+S^+ describes only double quantum coherence (DQC), whereas the cartesian product operator may be associated with several coherence orders, for example $2I_xS_x$ describes a linear combination of both DQC and zero quantum coherence (ZQC). The cartesian x and y components of a multiple quantum coherence are given by linear combinations of the shift or cartesian operators. For example, the ZQCs and DQCs of a two spin system can be described as follows

$$\begin{aligned}(\mathrm{ZQC})_x &= (2I_xS_x + 2I_yS_y) = (I^+S^- + I^-S^+)\\ (\mathrm{DQC})_x &= (2I_xS_x - 2I_yS_y) = (I^+S^+ + I^-S^-)\\ (\mathrm{ZQC})_y &= (2I_xS_y - 2I_yS_x) = \mathrm{i}(I^+S^- - I^-S^+)\\ (\mathrm{DQC})_y &= (2I_xS_y + 2I_yS_x) = -\mathrm{i}(I^+S^+ - I^-S^-)\end{aligned} \qquad (2.5)$$

On the basis of the operator formalism the selection of particular states using phase cycling of *rf* pulses in a NMR experiment can be rationalized. Coherences present in a experiment can be classified into their different orders or coherence levels which can be represented in a pictorial way (Fig. 1) to visualize the coherence transfer pathways in a experimental scheme [38, 39]. The

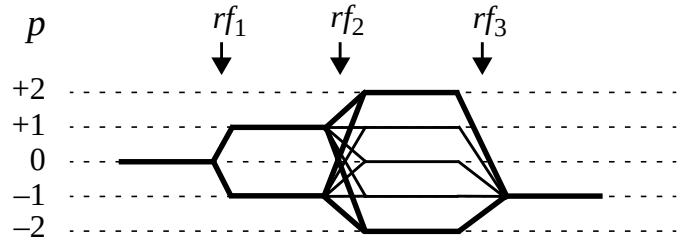

Fig. 1. Coherence level diagram. The coherence levels p are formally represented by products of the shift operators I^+ and I^- which are conserved during periods of free evolution. The application of radio-frequency pulses may transfer coherences from one order (level) to another. The positions of three pulses are indicated in the figure by vertical arrows labelled rf_1, rf_2 and rf_3. Thick lines represent the coherence pathway starting at the equilibrium state ($p = 0$) passing through single quantum coherences after the first pulse ($|p| = 1$), reaching double quantum coherences after the second pulse ($|p| = 2$) and ending as observable magnetization ($p = -1$) after the third pulse. Only single quantum coherences ($|p| = 1$) can be observed. The spectrometer detects only one of these two coherence levels which is usually assumed to be $p = -1$ [38] and hence all other coherence orders after the third pulse cannot be detected and therefore are not drawn. Thin lines indicate alternative pathways which have to be suppressed if only the pathway indicated by thick lines should contribute to the signal measured at the end of the sequence.

order of coherence p corresponds to the change q in the magnetic quantum number between the two connected states [28]. Hence for n coupled spins the maximal coherence level that can be reached is n. Free precession conserves the coherence order whereas pulses may cause coherences to be transferred from one order to another (Fig. 1). The sensitivity of a coherence to the phase of an *rf* pulse is proportional to its order, a q quantum coherence will experience a phase shift $\Delta\phi$ of an *rf* pulse as $q\Delta\phi$. If the pulse results in a change in the coherence order of Δp, the corresponding phase shift experienced by the affected coherence will be $-\Delta\phi\Delta p$. Proper phase cycling of consecutive *rf* pulses allows for selection of a specific succession of coherence levels that define a coherence pathway (Fig. 1). The concept of coherence transfer pathways clarifies the

role of phase cycling in NMR experiments and describes their action with a simple set of rules [21, 24, 38, 40]. A particular *rf* pulse can be designed to select a certain difference in coherence order $\Delta p \pm nN$ (n = 0, 1, 2, ..,) with a phase cycle comprising N phase steps $\Delta\phi$ of the same size equal to $360^o/N$. The N signals obtained must be summed together with the proper receiver phase $-k\Delta\phi\Delta p$ to compensate for the phase change experienced by the coherence, k takes on values {0, 1, 2, 3, ...}. An example for the design of a phase cycle using this recipe is given in Section 4.2.1 with the discussion of the double quantum filter. A detailed discussion of phase cycling can be found in most textbooks on NMR [*e.g.* 16, 21, 24, 26].

2.1.3 Descriptive representations of experimental schemes

An NMR experiment can be graphically described to a limited extent based on a classical physical model using populations and magnetization vectors in the rotating frame or based on quantum mechanical principles using the product operator formalism. Both descriptions find widespread applications for the discussion and development of NMR experiments. The different representations are discussed on the basis of the scheme shown in Fig. 2. The application of this experiment

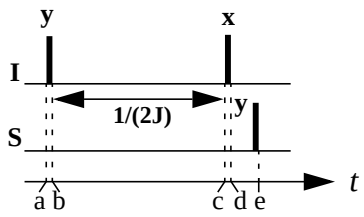

Fig. 2. Sketch of the experimental scheme used for the discussion of different representations shown in Fig 3. The black narrow bars indicate 90^o *rf* pulses, five time points on the time axis t are denoted by the letters a, b, c, d and e. The *rf* pulses applied on-resonance to the two species of nuclei I and S are indicated on the lines marked with the corresponding letters, a particular pulse acts only on one nuclear species. The scalar coupling between the two spins is J. The two pulses applied on spin I are separated by the time period $(2J)^{-1}$. The phases of the *rf* pulses are indicated with x or y at the top of the pulses, where x or y stand for the application of the B_1 field in the rotating frame along the positive x or y axis, respectively.

to a system of two scalar coupled spins I and S is described with four different representations in Fig. 3 for each of the five time points a to e. Fig. 3 represents energy level diagrams (E), the observable spectra (S), magnetization vector diagrams (V) and the notation in the product operator formalism (O) showing the cartesian and the shift operator basis. In Fig. 3 spins I and S are assumed to be proton and carbon nuclei, respectively, with the size of representative vectors proportional to the corresponding populations. But qualitatively the figure applies to all nuclei with spin $\frac{1}{2}$ and positive gyromagnetic ratio.

The experiment in Fig. 2 starts at time point a in thermal equilibrium (Fig. 3) where the populations on the upper P_u and the lower energy level P_l across a transition fulfil the Boltzmann distribution (Eq. (2.6)). Because ΔE in Eq. (2.1) is typically much smaller than kT we can approximate this exponential distribution by the first term in a Taylor expansion

$$P_u/P_l = \exp(-\frac{\Delta E}{kT}) \cong 1 - \frac{\Delta E}{kT} = 1 - \frac{\gamma\hbar B_o}{kT} \qquad (2.6)$$

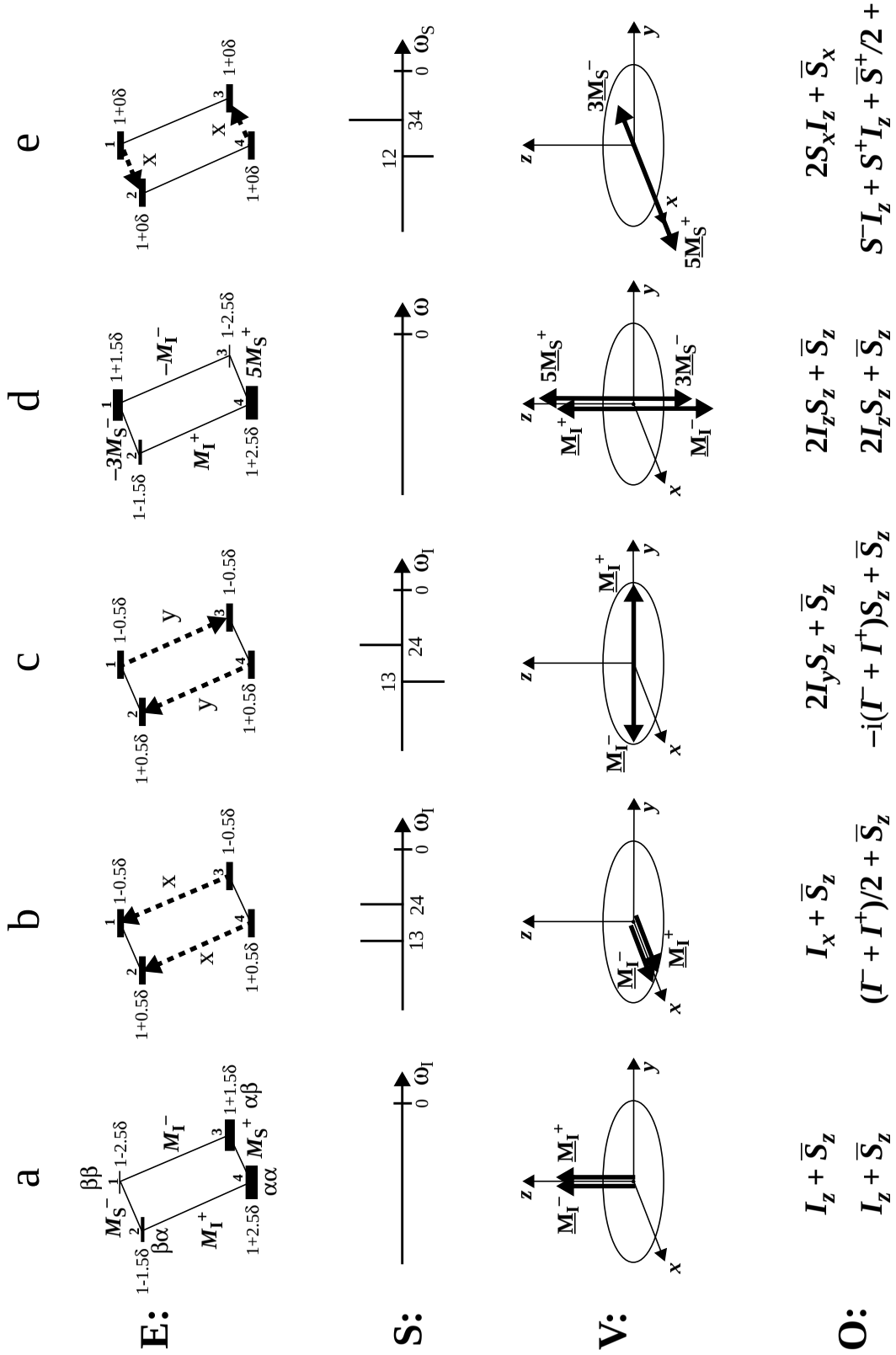
a
b
c
d
e
E:
S:
V:
O:
$I_z + \bar{S}_z$
$I_z + \bar{S}_z$
$I_x + \bar{S}_z$
$(I^- + I^+)/2 + \bar{S}_z$
$2I_yS_z + \bar{S}_z$
$-i(I^- + I^+)S_z + \bar{S}_z$
$2I_zS_z + \bar{S}_z$
$2I_zS_z + \bar{S}_z$
$2S_xI_z + \bar{S}_x$
$S^-I_z + S^+I_z + \bar{S}^+/2 + \bar{S}^-/2$

Fig. 3

Fig. 3. Different representations used for the description of NMR experiments illustrated for the experimental scheme shown in Fig. 2 using a two spin system consisting of a proton (*I*) and a carbon (*S*) nucleus with a scalar coupling $J>0$. The representations are qualitatively valid for all spins with a positive gyromagnetic value (Eqs. (2.2) and (2.6)). The labels a, b, c, d and e refer to the different time points indicated in Fig. 2. Four different representations are indicated. E: energy level diagrams, S: sketch of the observable spectrum, V: vector diagram and O: product operator formalism in the cartesian and in the shift operator basis. In E the spin states α and β associated with each energy level are indicated with the first character representing the proton spin and the second the carbon spin. The polarizations are indicated by *M* with the corresponding nucleus indicated as a subscript, the superscript plus or minus signs refer to the sign of the corresponding frequency of the components after excitation in the rotating frame (compare V). The populations of individual energy levels are normalized to one and deviations are given in units of δ with $\delta = \gamma_c \hbar B_o/(kT)$ (Eq. (2.6)) where γ_c is the gyromagnetic ratio for carbons. The ratio of 4 between the γ values of protons and carbons was used to represent populations. The coherences evolving after excitation have a "direction" (arrows) [16] and are labelled x and y for x and y phase, respectively. In the schematic stick spectra S the transitions are labelled according to the numbers of the connected energy levels. The spectra in S and the rotating frame in V are at the proton frequency at the time points a, b and c, at the proton and carbon frequency at time point d and at the carbon frequency at time point e. The vectors $\underline{M}$ in V are labelled with the same conventions as the polarizations in E. In the product operator representation the natural *S* spin magnetization is indicated by the operator $\overline{S}$.

where *k* is Boltzmann's constant and *T* the absolute temperature. With Eq. (2.1) the energies E_1, E_2, E_3, and E_4 of the four different energy levels in the system can be calculated

$$\begin{aligned} E_1 &= h(-\nu_I - \nu_S + J/2)/2 \\ E_2 &= h(-\nu_I + \nu_S - J/2)/2 \\ E_3 &= h(\nu_I - \nu_S - J/2)/2 \\ E_4 &= h(\nu_I + \nu_S + J/2)/2 \end{aligned} \qquad (2.7)$$

where ν_I and ν_S stand for the resonance frequencies of the *I* and *S* nuclei, respectively. The resonance frequencies of nuclei with positive gyromagnetic ratio γ such as protons and carbons are negative (Eq. (2.2)) and, hence, E_1 becomes the highest and E_4 the lowest energy (Fig. 3). For nuclei with a positive γ value the α state (spin $\frac{1}{2}$) has lower energy than the β state (spin $-\frac{1}{2}$). The polarizations M_I^+ and M_I^- are proportional to the energy differences (E_4-E_2) and (E_3-E_1), respectively, and they determine the intensity of the corresponding transitions 2<-->4 (24) and 1<-->3 (13). The consistent use of signs and transformation properties as presented in Fig. 3 may seem not to be of great importance and, indeed, has very often no direct experimental consequences. But there are situations where inconsistencies occur and the interpretation of data becomes confusing or wrong [31, 41].

Apart from the consistent illustration of different representations for the description of a NMR experiment, Fig. 3 demonstrates that the scheme shown in Fig. 2 transfers polarization from proton to carbon spins. At time point d the proton polarization M_I^- is inverted. As a consequence the populations across the carbon transitions 12 and 34 acquire a larger difference than at thermal equilibrium at time point a and, hence, the experimental scheme allows measurement of carbon spectra with higher sensitivity. Such polarization transfer experiments are extremely important in heteronuclear NMR experiments and are further discussed in Section 4.2.3.

2.1.4 Relaxation

Relaxation processes re-establish an equilibrium distribution of spin properties after a perturbation. After a disturbance, the non-equilibrium state decays in the simplest case exponentially characterized by the spin-lattice relaxation time T_1. Re-establishing thermal equilibrium requires changes in the population distribution of the spin states and lowers the energy of the spin system. Thus, it involves energy transfer from the spin system to its surroundings which is usually referred to as the lattice. Microscopically, relaxation is caused by fluctuating magnetic fields. Dynamical processes such as atomic or molecular motion produce fluctuating dipolar interactions and facilitate spin-lattice relaxation. The efficiency of the relaxation process depends on the extent of the overlap between the frequency spectrum of the motional process and the relevant resonance frequencies. This overlap is described by the spectral density function $J(\omega)$. Since $J(\omega)$ is the Fourier transform of the time correlation function describing the motion, its functional form depends on the mechanism of motion. An exponential correlation function with correlation time τ_c results in the spectral density function [16, 24, 29]

$$J(\omega) = \frac{2}{5} \cdot \frac{\tau_c}{1+\omega^2\tau_c^2} \tag{2.8}$$

Fig. 4 shows a plot of $J(\omega)$ as a function of the frequency ω for the three correlation times τ_c of 5 ns, 10 ns and 20 ns. These correlation times represent the motion of small, medium and large globular proteins in solution. In addition Fig. 4 illustrates that low frequency motions are espe-

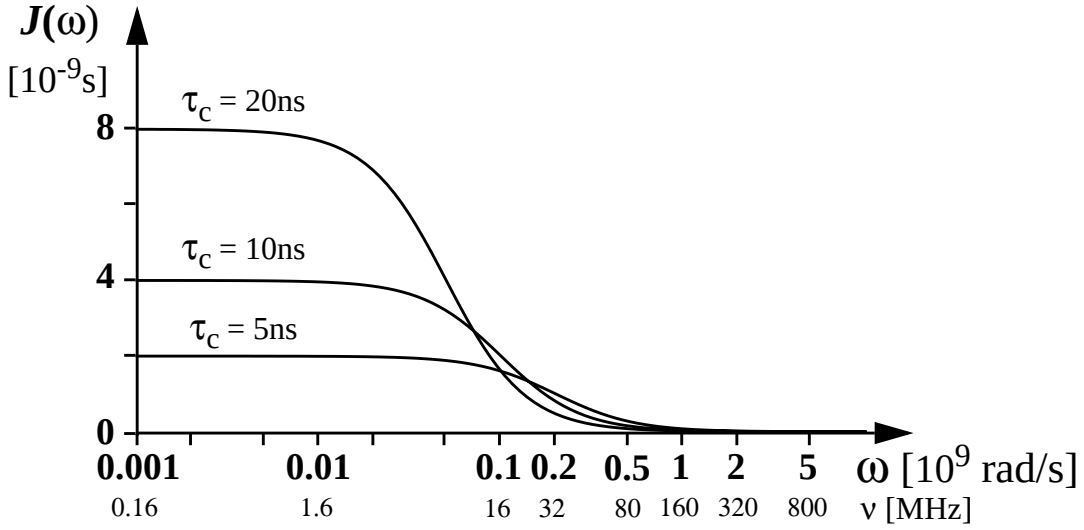

Fig. 4. Plot of the spectral density function $J(\omega)$ (Eq. (2.8) versus the frequency ω on a logarithmic scale. Three correlation times 5 ns, 10 ns and 20 ns are indicated which represent small, medium and large proteins. The frequency scale is given in units of rad/s and in MHz.

cially effective in NMR relaxation processes for proteins. Using the concept of spectral density functions the different behaviour of longitudinal relaxation and relaxation of transverse magnetization can be rationalized. When considering only relaxation due to fluctuating dipolar interactions caused by stochastic motion, the relaxation rate T_1^{-1} is proportional to $J(\omega_o)$ since only

stochastic magnetic fields in the transverse plane at the resonance frequency ω_o are able to interact with the transverse magnetization components bringing them back to the *z* axis. For frequencies larger than 25 MHz the values $J(\omega_o)$ decrease for the three increasing values of τ_c represented in Fig. 4. The longitudinal relaxation times, therefore, increase for increasing molecular weight of the protein. For very small molecules with very small τ_c the values $J(\omega_o)$ get smaller again leading to an increase of T_1 compared to the value for a τ_c of 5 ns (Eq. (2.8). The minimum T_1 value is obtained when $\omega_o\tau_c = 1$, *e.g.* at 600 MHz for a τ_c of 0.26 ns. Transverse relaxation shows a different dependence on the molecular weight of the molecule. T_2 relaxation not only depends on $J(\omega_o)$ but also on $J(0)$ since the *z* components of stochastic magnetic fields (zero frequency) reduce the phase coherence of transverse magnetization components which consequently sum up to a smaller macroscopic magnetization. Since $J(0)$ monotonously increases with increasing correlation times (Eq. (2.8), Fig. 4) T_2 decreases monotonously with increasing molecular weight. Short T_2 values reduce the performance of NMR experiments with large molecules. However, relaxation depends not only on the size of a molecule but also on its internal motions. Two molecules with the same molecular weight may show quite different relaxation behaviour depending on their particular internal motions.

2.1.5 Through-bond correlations

The magnetic dipole-dipole interaction describes the effect of the local magnetic fields associated with the magnetic moments of surrounding nuclei. Two mechanism contribute to this effect: the "direct" (through-space) coupling and the "indirect" spin-spin coupling or *J* coupling transmitted *via* polarization of bonding electrons. The complete analysis of protein spectra is based on interactions between different spins, either mediated by electrons in through-bond correlations or by direct interactions through space. Through-bond correlations group individual spins into spin systems [15] which are characteristic for individual amino acids. In proteins couplings over more than three chemical bonds are usually not observed. Consequently only spin systems for amino acid types can be obtained for unlabelled or ^{15}N labelled proteins but the sequential arrangement of these spin systems relies on through-space correlations [5, 6] which may be ambiguous for larger proteins. The efficiency of through-bond correlations depends on the size of the coupling constants involved. Heteronuclear coupling constants often are much larger than proton-proton couplings (Fig. 5). The use of heteronuclear coupling constants requires the protein to be labelled with ^{15}N and/or ^{13}C isotopes. With ^{13}C, ^{15}N doubly labelled proteins spin systems of individual amino acid residues can be connected *via J* couplings across the peptide bond. Based on heteronuclear couplings a complete assignment can be obtained from through-bond correlations alone. Fig. 5 summarizes some typical coupling constants found for nuclei in proteins. A wide range of experiments for the determination of homo- and heteronuclear scalar coupling constants in proteins exist. An excellent survey of these methods can be found in a recent review [42].

Two principally different mechanisms for the through-bond correlation of spins are used. Either individual spin pairs are correlated or all spins in a spin systems interact simultaneously. The first case is often referred to as a COSY-type and the second as TOCSY-type correlation. TOCSY stands for total correlation spectroscopy [43] also known under the acronym HOHAHA for homonuclear Hartmann-Hahn transfer [44]. Both types of correlation can transfer magnetization between two nuclei. Thus the sensitivity of a nucleus can be enhanced when the experiment starts with the polarization of a nucleus of a different species with a higher gyromagnetic ratio (Fig. 2 and Fig. 3). Polarization transfer based on a COSY-type sequence was given the acronym INEPT [45] which stands for insensitive nuclei enhanced by polarization transfer. Polarization transfer

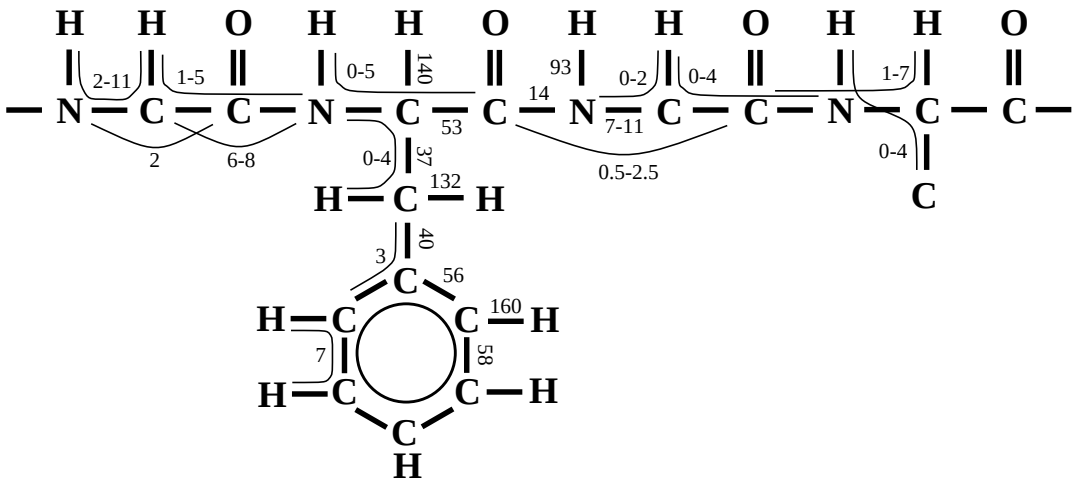

Fig. 5. Typical absolute values for coupling constants and their range in Hertz. If the variation is less than 10% of the maximal value single average values are given otherwise the range is indicated by the maximal and the minimal value. One bond coupling constants are written along the bond, for multiple bond coupling constants a line drawn along the chemical bonds connects the two coupled nuclei.

based on a TOCSY-type sequence usually is referred to as HEHAHA (heteronuclear Hartmann-Hahn) experiment (Section 4.2.3).

The COSY-type correlation can easily be rationalized using the product operator formalism for two scalar coupled spins I and S (Eq. (A.2.2) in the Appendix). Transverse I_y magnetization will evolve into anti-phase magnetization of the form $2I_xS_z$ due to scalar coupling. A 90^o *rf* pulse with phase *y* on both spins transforms this operator product into $2I_zS_x$ which can evolve into the observable operator S_y. The crucial element in a COSY-type transfer is the 90^o *rf* pulse acting on an anti-phase state. If the two nuclei belong to two different nuclear species the polarization transfer from spin I to spin S (Fig. 3) will change the sensitivity of the spin S spin by the ratio γ_I/γ_S of the gyromagnetic ratios.

In a homonuclear TOCSY-type transfer a strong *rf* field is applied to one nuclear species. Viewed in the rotating frame this field locks the spins along the axis it is applied. In this spin-locked state individual precession around B_o is suppressed and replaced by a collective precession with the frequency of the applied *rf* field. Without their characteristic precession frequencies the spins lose their individuality and can no longer be distinguished and behave as part of a strongly coupled spin system. The product operator formalism cannot describe such a state and an analysis is only possible using a quantum mechanical treatment. A homonuclear two spin system with scalar coupling J evolves under spin-locking for a period τ_m from the state I_x as follows [43]:

$$I_x \text{ ----> } I_x\,[1 + \cos(2\pi J\tau_m)]/2 + S_x\,[1 - \cos(2\pi J\tau_m)]/2 + [I_yS_z - I_zS_y]\,\sin(2\pi J\tau_m) \qquad (2.9)$$

For $\tau_m = (2J_{IS})^{-1}$ complete in-phase magnetization transfer from I_x to S_x will occur. For more than two coupled spins different coupling constants will govern the transfer and complete transfer from one spin to another is usually not possible. The theoretical evaluation leading to Eq. (2.9) does not consider offset effects of *rf* pulses. When the effective fields for two nuclei are not

aligned (Eqs. (A.1.3) and (A.1.4) in the Appendix) the effective *J* coupling during the mixing sequence is reduced resulting in a slower transfer. In addition to magnetization transfer through bonds TOCSY mixing sequences transfer magnetization through space as discussed in the next section. This pathway requires special attention only for very sensitive nuclei such as protons and can safely be neglected for all other nuclei. Detailed descriptions of the foundations of the TOCSY experiment can be found in literature with both experimental [46] and theoretical treatments [43, 47].

In the more general case of the heteronuclear TOCSY, magnetization is transferred between nuclei of different species. In this situation two *rf* fields B_{1I} and B_{1S} at two different nuclear resonance frequencies have to be applied, with $B_{1I} = \gamma_I\omega_I$ and $B_{1S} = \gamma_S\omega_S$. As in the HOHAHA experiments the spins must experience the same magnetic field strength to loose their individuality and to form a strongly coupled system. Setting B_{1I} and B_{1S} equal one obtains the well known Hartmann-Hahn condition [16, 19, 48] which must be fulfilled to obtain a heteronuclear TOCSY transfer:

$$\gamma_I\omega_I = \gamma_S\omega_S \tag{2.10}$$

If for example *I* stands for a proton and *S* for a ^{15}N nucleus the locking *rf* field applied to ^{15}N has to be almost ten times larger than the one applied to protons (Table 1). Based on a quantum mechanical treatment the transformation properties of the operator I_x of a heteronuclear two-spin system submitted to a HEHAHA sequence can be formulated in analytical form [16, 24]

$$I_x \text{ --->} I_x\,[1 + \cos(\pi J\tau)]/2 + S_x\,[1 - \cos(\pi J\tau)]/2 + [I_yS_z - I_zS_y]\,\sin(\pi J\tau) \tag{2.11}$$

where *J* stands for the heteronuclear coupling constant between the spins *I* and *S*. For a full transfer of the magnetization in a HEHAHA experiment the mixing time τ_m must be $1/J_{IS}$ which corresponds to double the duration compared to the homonuclear transfer (Eq. (2.9)).

2.1.6 Through-space correlations

A nucleus with a spin different from zero generates a magnetic dipolar field proportional to its magnetic moment. As the molecule tumbles in solution, this field fluctuates and constitutes a mechanism of relaxation for nearby spins. Since the dipole-dipole interaction involves a pair of spins, four states can occur for a system with two spins $\frac{1}{2}$. Due to the double and zero quantum transitions which are possible in such a system, the longitudinal relaxation process for the two spins *I* and *S* are coupled [49] and the expectation values $<I_z>$ and $<S_z>$ describing the *z* magnetization fulfil the equation

$$\begin{aligned} d/dt(<I_z> - I_o) &= -\rho_N\,(<I_z> - I_o) - \sigma_N(<S_z> - S_o) \\ d/dt(<S_z> - S_o) &= -\rho_N\,(<S_z> - S_o) - \sigma_N(<I_z> - I_o) \end{aligned} \tag{2.12}$$

where ρ_N stands for the longitudinal relaxation rate constant of the two spins *I* and *S* of the same nuclear species, σ_N for the cross relaxation rate constant and I_o or S_o are the equilibrium magnetizations. The coupling of the relaxation of the two nuclei will alter the magnetization of one spin when the other spin is not in its equilibrium state. For example, when the equilibrium value S_o is selectively disturbed leading to a deviation ΔS from S_o then the *I* magnetization will change from I_o with a initial rate proportional to $\sigma_N\Delta S$ (Eq. (2.12). The following expression can be derived

for σ_N and ρ_N using two spins of the same species without scalar coupling and with an internuclear distance r [50]:

$$\sigma_N = \frac{K}{r^6} (6J(2\omega_o) - J(0)) \tag{2.13}$$

$$\rho_N = \frac{K}{r^6} (J(0) + 3J(\omega_o) + 6J(2\omega_o)) \tag{2.14}$$

$$K = \left(\frac{\mu_o}{4\pi}\right)^2 \cdot \frac{h^2\gamma^4}{16\pi^2} \tag{2.15}$$

These expressions are valid in the case of isotropic tumbling and dipolar relaxation. σ_N can take on positive and negative values depending on the value of the spectral density function in Eq. (2.8) (Fig. 4) and has a zero crossing (Fig. 6). For globular proteins measured at high magnetic fields σ_N is negative. For protons K equals $1.424 \cdot 10^5$ nm^6/s^2. For example in a globular protein with a rotational correlation time of 10 ns, σ_N becomes approximately -10 s^{-1} for two protons at a distance r of 0.2 nm and $\sigma_N = -0.04$ s^{-1} for $r = 0.5$ nm. Nuclear Overhauser enhancement (NOE) experiments make use of the cross relaxation between spins and allow detection of nuclei which are close in space, in practice at a maximal distance of about 0.5 nm for protons in a globular protein. In a system with more than two spins consecutive cross relaxation can occur leading to so called spin diffusion [51] where two distant spins exhibit a larger apparent cross relaxation due to the contributions of the intervening spins. This effect complicates the derivation of distances from NOE measurements. Since the initial NOE is proportional to σ_N spin diffusion becomes more important for larger proteins which exhibit a longer rotational correlation time τ_c (Fig. 6). Practical implementations exploiting cross relaxation use the NOESY segment discussed in Section 4.2. 2.

Based on the observation of cross relaxation between I_z and S_z states one may expect a similar effect with transverse magnetization. In general, a net magnetization transfer between transverse magnetization components does not occur because the spins precess with different frequencies and the continuously changing phase relationship between the corresponding magnetization vectors prevents the accumulation of a net transfer of magnetization. The situation changes when different spins are forced to precess at the same frequency by applying a strong *rf* field. With the individual precession frequencies removed a net transfer can be established which couples the transverse relaxation process for two spins I and S. In analogy to the calculation of σ_N a cross relaxation rate constant, σ_R, and a relaxation rate constant, ρ_R, can be obtained [50, 52]:

$$\sigma_R = \frac{K}{r^6} (2J(0) + 3J(\omega_o)) \tag{2.16}$$

$$\rho_R = \frac{K}{2r^6} (5J(0) + 9J(\omega_o) + 6J(2\omega_o)) \tag{2.17}$$

The NOE between spin-locked transverse magnetization components is usually referred to as NOE in the rotating frame (ROE). Originally the ROE experiment was called CAMELSPIN [53], but was later renamed ROESY for the two-dimensional ROE experiment [54]. Fig. 6 illustrates that the cross relaxation rate σ_R does not have a zero crossing and that for molecules with a correlation time τ_c larger than 0.05 ns σ_R is larger than σ_N. A detailed theoretical derivation of homonuclear cross relaxation in the rotating frame can be found in an excellent review [52] and a number of textbooks [*e.g.* 16, 24, 26, 50].

Since ROE and TOCSY mixing sequences, both use a spin-lock field to suppress the individual precession frequencies of transverse magnetization components special care is required in the

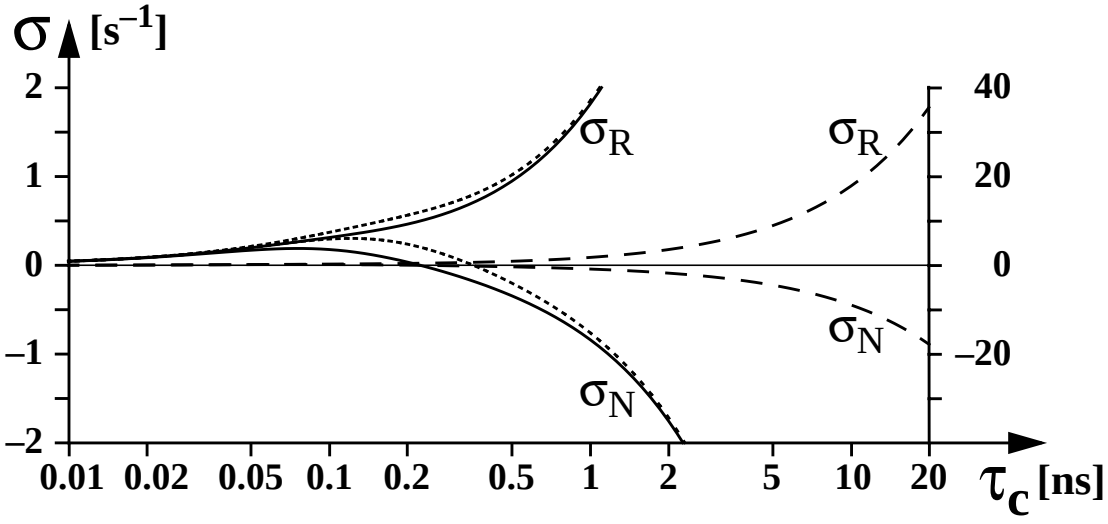

Fig. 6. Plot of cross relaxation rates σ versus the rotational correlation time τ_c for a two spin system. σ is given for the NOE in the laboratory frame denoted with σ_N and in the rotating frame, σ_R, for two spectrometer frequencies: 800 MHz indicated with solid lines and 500 MHz drawn with dotted lines. For these curves, the scale for σ on the left hand side of the figure applies. The dashed lines show σ_N and σ_R on a 20-fold smaller vertical scale shown on the right hand side. On this scale the curves for the two field strength are indistinguishable. For the calculation the equations (2.8), (2.13), (2.15) and (2.16) were used assuming two protons with a constant internuclear distance of 0.2 nm.

implementation to separate the two effects (Section 4.2.1). Although there are experimental implementations which minimize the simultaneous occurrence of both effects, a strict separation is not possible and both processes can contribute to correlations between scalar coupled nuclei. Nevertheless ROE and TOCSY type mixing sequences find widespread applications because the residual interference between them can in many practical cases be distinguished since the two effects generate signals with different signs.

Both the NOE and ROE enhancements for short mixing times are proportional to the cross relaxation rate which for globular proteins is dominated by the spectral density function at zero frequency, $J(0)$, and therefore from Eqs. (2.13) and (2.16) $\sigma_R \cong -2\sigma_N$. This relation indicates that the ROE effect builds up signal with increasing mixing time twice as fast and in the opposite direction from NOE spectra. When results from ROE and NOE spectra are to be directly compared the mixing time for the ROE experiment is often chosen half as long as for the NOE experiment. Both ROE and NOE experiments not only detect cross relaxation but also magnetization transfer by chemical or conformational exchange. Whereas the sign for the NOE and the ROE effect may be different this is not the case for exchange contributions which always have opposite sign compared to the ROE effect. This allows a separation of exchange contributions from NOE effects.

2.2 Radio frequency pulses

2.2.1 Rectangular pulses

A NMR experiment consists of a series of *rf* pulses and delays, the pulse sequence, followed by the measurement of the voltage induced by the resulting magnetization in a *rf* coil (Section 3.5.1). A delay specifies a time period during which no external *rf* field is applied and the nuclear spin states evolve due to their intrinsic properties (chemical shift, scalar coupling and relaxation). A pulse represents a time period during which *rf* is delivered to the coil in the probe. Four parameters describe a *rf* pulse: frequency, phase, duration and strength. The frequency of the pulse is often called the carrier frequency since, generally, it is identical to the frequency used to demodulate the detected NMR signal. For a rectangular pulse the strength stays constant during its application. The magnetic field strength applied during such a pulse is often given in frequency units γB_1 which can be obtained with Eq. (2.3) by setting the pulse flip angle to 2π for a 360^o pulse with the corresponding pulse length τ_{360}:

$$\frac{\gamma B_1}{2\pi} = \gamma B_1 = \frac{1}{\tau_{360}} \tag{2.18}$$

For example, a 90^o pulse with a duration of 12.5 μs is produced by a field strength γB_1 of 20 kHz.

Ideally a *rf* pulse applied to a given nuclear species will rotate all magnetization components irrespective of their individual resonance frequencies by the same flip angle β about the axis in the rotating frame defined by the phase of the pulse. However, the performance of a real *rf* pulse degrades with increasing offset of the nuclear precession frequencies from the applied *rf* frequency. The precession axis introduced by a *rf* pulse applied off-resonance deviates from the direction of the B_1 field of the pulse (see Appendix). Whereas for a 90^o excitation pulse satisfactory performance can be obtained over a wide bandwidth, the efficiency of a 180^o pulse degrades rather rapidly. Fig. 7 shows excitation profiles for 180^o and 90^o pulses in dependence of the offset frequency. Best use of these excitation profiles can be made when the carrier frequency sits in the middle of the spectral range of interest. A 90^o pulse applied to *z* magnetization brings most magnetization into the transverse plane when the offset frequency ν_{off} fulfils the condition $\nu_{off} < \gamma B_1$. However, the magnetization acquires an offset dependent angle ε to the direction it would reach after an ideal 90^o pulse with duration τ_{90}. This angle ε can be calculated to be $4\tau_{90}\nu_{off}$ in units of radians [16, 24, 26].

A further consequence of the non-ideal behaviour of *rf* pulses are specific offset frequencies at which the pulse does not perturb the resonances. This feature can be used to excite one group of resonances while selectively avoiding excitation of another group. A technique that finds frequent applications in heteronuclear experiments involving carbon nuclei where carbonyl carbons and aliphatic carbons are excited separately. Using the Bloch equations (see Appendix) the *k*-th null in the excitation profiles can be calculated for a 90^o pulse with duration τ_{90} to be at a frequency ν_{90} and for a 180^o pulse with duration τ_{180} at a frequency ν_{180} from the carrier frequency:

$$\nu_{90} = \pm\sqrt{k^2 - \frac{1}{16}} \,/\, \tau_{90} \tag{2.19}$$

$$\nu_{180} = \pm\sqrt{k^2 - \frac{1}{4}} \,/\, \tau_{180} \tag{2.20}$$

For a 90^o pulse the first null is at $\nu_{90} = \pm 0.97/\tau_{90}$ and for a 180^o pulse at $\nu_{180} = \pm 0.87/\tau_{180}$.

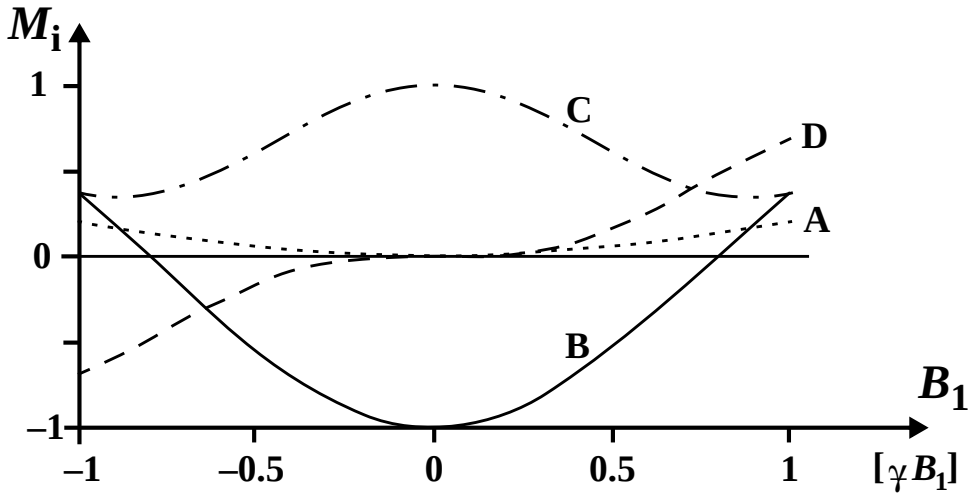

Fig. 7. Excitation profiles of *rf* pulses represented by the normalized magnetization M_i plotted against the offset given in units of γB_1 where B_1 is the applied field strength. (A) M_z after a 90^o excitation pulse and (B) M_z after a 180^o inversion pulse applied to *z* magnetization. (C) M_x after a 180^o refocusing pulse with phase x applied to *x* magnetization. (D) Same as (C) but M_y is shown.

Typically several 180^o pulses occur in a pulse sequence and the signals created by their non-ideal behaviour may limit the spectral quality. With a phase cycling scheme, EXORCYCLE [55], magnetization components not inverted by the 180^o pulse and those which underwent a coherence transfer due to off resonance effects can be removed from the detected signal. The EXORCYCLE consists of a 4-step phase cycle where the phase of the 180^o pulse changes according to the scheme x, y, –x, –y together with the receiver phase cycling through x, –x, x –x.

Many applications require the inversion of *z* magnetization. In this case simple composite pulses exhibit much broader inversion profiles than a single 180^o pulse. A composite pulse based on a 180^o pulse with phase y embraced by 90^o pulses with phase x, in short notation $90_0\,180_{90}\,90_0$, shows more than 80% inversion over a bandwidth of $\pm\gamma B_1$ [56]. The composite pulse $90_0\,225_{90}\,90_0$ where the 180^o pulse is replaced by a 225^o pulse results in even better inversion of more than 98% however at the cost of a smaller bandwidth of $\pm 0.7\gamma B_1$. Analogous simple composite pulses for improved refocusing of transverse magnetization do not exist [57].

When pulses or more complex pulse trains with low power are applied selectively to only a small frequency range in a spectrum the signals at an offset $\Delta\nu$ far from the irradiation frequency can still be significantly affected. These off-resonance or non-resonant effects can lead to a phase shift ϕ_{nr} and a rotation ρ of the evolving magnetization and depend on the strength $\nu_2(t) = \gamma B_2(t)$ of the applied magnetic field $B_2(t)$ [34, 35]. The rotation ρ is towards the positive *z* axis around an axis perpendicular to the axis along which the *rf* pulse is applied. Both ϕ_{nr} and ρ depend on the length τ_p of the pulse train applied and on the average of the square of the field strength, $<\nu_2^2(t)>$, in addition ρ is proportional to the average of the field strength:

$$\phi_{nr} = \pi \langle \nu_2^2(t) \rangle \tau_p/\Delta\nu \tag{2.21}$$

$$\rho = \pi \langle \nu_2^2(t) \rangle \langle \nu_2(t) \rangle \tau_p/(\Delta\nu)^2 = \phi_{nr} \langle \nu_2(t) \rangle/\Delta\nu \tag{2.22}$$

In these equations ϕ_{nr} and ρ are given in units of radians. Eq. (2.21) and (2.22) exhibit clear differences between ρ and ϕ_{nr}. The rotation ρ is always smaller than the phase shift ϕ_{nr} and when the average strength of the applied field $\langle \nu_2(t) \rangle$ is zero then the rotation ρ, but not ϕ_{nr}, vanishes completely, a situation encountered with composite pulse decoupling where $\langle \nu_2(t) \rangle = 0$ due to the applied phase cycling schemes. A typical numerical example relates to the decoupling of alpha carbon resonances from carbonyl carbons which are separated by $\Delta\nu = 18000$ Hz on a 600 MHz NMR spectrometer. The application of an 8 ms long, low power WALTZ decoupling sequence to carbonyl carbons using a 1 kHz decoupling field strength results in $\phi_{nr} = 1.4$ rad (80^o) and $\rho = 0$. Using instead of WALTZ a rectangular 180^o pulse at the carbonyl frequency with its sixth null at 18000 Hz (Eq. (2.20)) to refocus the effect of the carbonyl couplings, the values change to $\phi_{nr} = 0.13$ rad (7.5^o) and $\rho = 0.6^o$.

In the course of a multidimensional NMR experiment selective decoupling may be applied during an evolution time which is incremented. In this situation τ_p linearly increases and considering Eq. (2.21) it becomes clear that the time dependent phase ϕ_{nr} will manifest itself as a frequency shift ν_{nr}:

$$\nu_{nr} = \langle \nu_2^2(t) \rangle/2\Delta\nu \tag{2.23}$$

With the numerical example given above using WALTZ decoupling, the frequency shift ν_{nr} becomes 27.8 Hz. The numerical examples show that the non-resonant effects described by ϕ_{nr} and ρ may cause severe signal loss and care has to be taken to correct for their influence. Four different procedures can be envisaged to compensate for non-resonant effects [35]:

1. Adjusting the phase and flip angle of the pulse directly following or preceding the occurrence of non-resonant effects.
2. A phase error occurring during an evolution time can be corrected by applying a phase correction after Fourier transformation.
3. Compensation by modulating the amplitude of the pulse train with a cosine function which results in the application of the disturbing field at $+\Delta\nu$ and $-\Delta\nu$ and thereby cancelling the effects at the frequency of interest.
4. Applying the disturbing field twice, once before and once after a non-selective 180^o pulse and thereby refocussing the adverse effects.

2.2.2 Amplitude modulated pulses

Modulating the amplitude of a pulse permits the design of specific excitation profiles. Since the shape of a pulse and its excitation profile are not related by a Fourier transformation [16] more elaborate procedures must be used to find the optimal pulse shape based on a desired excitation profile. A large selection of pulse shapes have been developed and characterized [58]. From a given pulse shape the excitation profile can be calculated by integrating the Bloch equations given in the Appendix. Software packages on commercial spectrometers include corresponding routines (Bloch simulator) which help to choose the appropriate shape for a specific experiment

and to determine its parameters. In general a good amplitude modulated pulse should have an adequate frequency selectivity, uniform excitation, uniform phase behaviour and a short duration. Some of these desired properties contradict each other. Improving the selectivity, for example, tends to increase the pulse duration which should be kept as short as possible to counteract relaxation losses. During the application of a selective pulse, the magnetization components of interest accumulate an offset-dependent phase error. If the phase error is approximately linear across the excitation bandwidth it can be refocused by a non-selective 180^o pulse after a suitable delay within or after the selective pulse [59]. Far from its irradiation frequency a selective pulse may introduce non-resonant phase and amplitude errors as described by Eqs. (2.21) and (2.22). These deficiencies can be corrected using the same methods as described for rectangular pulses in Section 2.2.1.

The performance of an amplitude modulated pulse depends on the initial state of the magnetization. A selective 180^o pulse that provides good inversion properties for longitudinal magnetization in general does not perform well as a 180^o refocusing pulse for transverse magnetization. For this reason, some shapes of pulses, for example the BURP pulses [60], are grouped into families with a member for excitation, inversion and refocusing. The most frequently used shaped pulses are Gaussian, sinc with no or one pair of side lobes, Gaussian cascades [61] which are based on individual Gaussian shaped pulses, and pulses of the BURP family [60].

The application of amplitude modulated pulses in a pulse sequence requires all stages of the transmitter pathway of the spectrometer to be linear, otherwise the shape and hence the excitation profile deviate from the one selected. The direct determination of the pulse length of an amplitude modulated pulse can be rather tedious. In this situation the use of a Bloch simulator program which integrates the Bloch equations (Eq. (A.1.1)) seems more efficient for the determination of the parameters of a shaped pulse by using the known parameters of a rectangular 90^o pulse to determine the field strength of a given power setting. A prerequisite for such calculations is the linearity of the transmitter channel. In addition amplitude modulated pulses can be rather sensitive to *rf* inhomogeneity of the coil in the probe and therefore require good *rf* homogeneity for best performance.

2.2.3 Amplitude and phase modulated pulses

A pulse excites a spectral range around its irradiation frequency, however some experimental techniques require the pulse to excite at a frequency different from this position. For example in the middle of a period of free precession a selective 180^o pulse may need to be applied to the amide protons to decouple them from the alpha protons. If the carrier is to remain on the water resonance this requires a homonuclear off-resonance selective pulse. Off-resonance pulses have the advantage over switching the carrier frequency in that the latter method generates a phase shift which must be taken into account and complicates the phase setting of subsequent pulses applied to the precessing magnetization. The center of excitation of a pulse cannot only be changed by changing its frequency but also by changing its phase during the application. Two types of phase modulated pulses can be distinguished: pulses shifted off-resonance by a fixed frequency and pulses where the frequency is swept during their application. A pulse with a fixed off-resonance frequency shift ν_{off} during the application can be obtained by linearly increasing the pulse phase $\Phi(t)$ with time while keeping the carrier frequency fixed at ν_o:

$$\cos(2\pi\nu_o t + \Phi(t)) = \cos(2\pi\nu_o t + (\Phi_o + 2\pi\nu_{off}\, t)) \qquad (2.24)$$

The increment per unit time depends on the required offset frequency ν_{off} from the carrier frequency ν_o. A positive phase increment will shift the frequency to higher values, decrementing the phase lowers the effective frequency of the pulse. For example, amide protons or carbonyl carbons resonate at a higher absolute frequency than methyl resonances of protons or carbons, respectively. The time point $t = 0$ sets the reference phase Φ_o for the off-resonance pulse. Any further pulse on transverse magnetization of the same nuclear species during the pulse sequence at a later time point T will have the phase $\Phi(T)$ which in general deviates from Φ_o. The performance of pulses which invert z magnetization will usually be independent of $\Phi(T)$. However, off-resonance pulses that create or act on transverse magnetization require the phase $\Phi(T)$ to be adjusted properly otherwise signal may be lost. $\Phi(T)$ can be calculated on the basis of Eq. (2.24) and for example the proper time chosen where $\Phi(T) = \Phi_o$.

When the phase $\Phi(t)$ in Eq. (2.24) depends non-linearly on the time t the effective frequency changes during the pulse. An important group of pulses using frequency sweeps during their application are the adiabatic pulses. These pulses excite, invert or refocus magnetization over a very wide frequency range at the cost of a longer pulse duration and a phase dispersion across the excitation bandwidth. In applications where such pulses excite or invert magnetization they are robust to *rf* inhomogeneities but not when applied for refocusing [62]. An additional feature makes adiabatic pulses very attractive: doubling the *rf* field strength of the pulse quadruples the bandwidth covered [62]. A distinct advantage over conventional pulses which excite a bandwidth proportional to the strength of the pulse.

The concept of adiabatic pulses can be understood with the help of a description in the rotating frame. With the applied radio frequency field B_1 far above resonance the effective field B_{eff} corresponds to the residual magnetic field B_z (Eq. (A.1.3) and Fig. A1 in the Appendix) and the magnetization M stays aligned along the positive z axis. Sweeping the frequency of B_1 towards resonance will tip away B_{eff} from the z axis towards the transverse plane. For a sufficiently slow sweep the magnetization M stays aligned with the changing direction of the effective field. At resonance B_{eff} and M lie in the transverse plane. As the frequency of the exciting field B_1 passes through resonance and subsequently is swept to frequencies much lower than resonance, the magnetization M moves on towards the negative z axis (Eqs. (A.1.3) and (A.1.4)). For M to follow B_{eff} the adiabatic passage condition must be fulfilled [29]:

$$|d\Theta/dt| << \gamma B_{eff} \quad \text{with} \quad B_{eff} = (B_1^2(t) + B_z^2(t))^{1/2} \tag{2.25}$$

where B_z represents the offset from the resonance frequency and Θ describes the angle between the effective field and the z axis (Eq. (A.1.4)). With Eq. (2.25) and Eq. (A.1.4) one finds that the critical stage of any adiabatic sweep is the point where B_1 sweeps through resonance for a given magnetization component resulting in the relation

$$dB_z(t)/dt << \gamma B_1^2(t) \tag{2.26}$$

In addition to the condition described in Eq. (2.26) adiabatic passage requires that no relaxation occurs during the sweep period. In practical implementations the field cannot be swept starting at an infinitely large offset, however when choosing a finite starting value the effective field and the magnetization M are not aligned. Consequently M precesses around B_{eff} which degrades the performance of adiabatic pulses. To reduce this initial precession the starting angle Θ_o must be as small as possible. For small values of Θ one finds with Eq. (A.1.4)

$$\Theta = B_1/B_z \tag{2.27}$$

Based on Eq. (2.27) small values of Θ require large initial offsets for the start of the sweep. For an angle Θ corresponding to 1^o (0.0175 rad) and with γB_1 = 2 kHz an offset of at least 115 kHz is necessary. Eq. (2.27) suggests an alternative approach to reduce the initial offset substantially. If the sweep starts with an amplitude of B_1 at zero and is smoothly increased to its nominal value, then the offset where the sweep must start, can be reduced making adiabatic sweeps more efficient [62]. The same consideration for the end of the adiabatic sweep leads to the conclusion that the amplitude of B_1 should be smoothly reduced to zero.

As long as Eq. (2.26) stays fulfilled, the time dependent phase $\Phi(t)$ of the pulse can have any functional form. For simplicity very often linear sweeps are applied (Eq. (2.28)). With the total sweep range F and the total duration of the sweep τ_s the change of B_z per unit time (dB_z/dt) becomes $2\pi F/\gamma\tau_s$. Linear sweeps result in a quadratic time dependence for the phase $\Phi(t)$ of the constant frequency ν_o during the application of an adiabatic pulse:

$$\cos(2\pi\nu_o t + \Phi(t)) = \cos(2\pi\nu_o t + (\Phi_o + (2\pi F/\gamma\tau_s)\, t^2)) \tag{2.28}$$

Most applications of adiabatic pulses use single inversion pulses or trains of inversion pulses in decoupling sequences. When used to refocus transverse magnetization, their inherent long execution time may cause problems with fast relaxing magnetization as well as with evolution due to scalar couplings which may modulate the signals. On the other hand, depending on the chemical shift range of scalar coupled nuclei, partial decoupling may be achieved during the adiabatic pulse [63, 64]. Applications for refocusing are not yet very common but their applicability has been demonstrated [63, 65, 66].

2.3 Magnetic field gradients

Pulsed magnetic field gradients (PFGs) have been used in NMR spectroscopy for more than 30 years to study the diffusion of molecules in solution [67, 68]. However, PFGs became a routine tool in high resolution NMR in solution [69–73] only since the introduction of actively shielded gradient coils which offer short recovery times (Section 3.5.2) for the re-establishment of the very homogeneous magnetic field after the application of a PFG. The resonance frequency of nuclei placed in a magnetic field gradient becomes dependent on their spatial location. A linear PFG with the strength G per unit length along the z direction produces the following dependence of the resonance frequency $\omega(z)$ on the z coordinate

$$\omega(z) = \omega_o + \gamma G z \tag{2.29}$$

where ω_o is the resonance frequency without the application of a PFG. The evolution of the operators used to describe an NMR experiment (Section 2.1.2) become dependent on the vertical position in the sample. Using the shift operator basis the following transformations are obtained due to the action of a gradient pulse applied for a duration τ:

$$\begin{aligned} I^- &\dashrightarrow I^- e^{i\gamma G z \tau} \\ I^+ &\dashrightarrow I^+ e^{-i\gamma G z \tau} \\ I_z &\dashrightarrow I_z \end{aligned} \tag{2.30}$$

In these transformation rules the evolution due to chemical shift and *J* coupling are not included. The phase factor γGz describing the spatial dispersion of the resonance frequencies depends on the gyromagnetic ratio γ which makes the action of a gradient less efficient for nuclei with a small γ. For example, applying an identical gradient on transverse proton and nitrogen magnetization will result in a spread of resonance frequencies across the sample which is ten times larger for proton than for nitrogen nuclei. Eq. (2.30) describes how the evolution of magnetization components depends on the *z* coordinate. However, the magnitude of the macroscopic magnetization *M* will be the integral over the sample length *L* which results in the following relationship

$$M = \frac{\sin(\gamma G\tau L/2)}{\gamma G\tau L/2} = \mathrm{sinc}(\gamma G\tau L/2) \qquad (2.31)$$

The sinc function in Eq. (2.31) has a damped oscillatory behaviour and is zero only at specific values. In between the zero crossings the detectable signal can reach appreciable values and can interfere with the performance of the experiment requiring the value for $\gamma G\tau L$ to be optimized. For example, a moderate gradient with a duration of 1 ms and a strength of 0.1 T/m applied to proton magnetization using a typical commercial probe will show a maximum signal recovery between the first and second zero crossing of about 0.5% of the original intensity which, for example, results in a substantial residual signal for the solvent resonance.

Pulsed magnetic field gradients find three main applications: (i) spatial encoding of coherences, (ii) elimination of unwanted coherences and (iii) selection of coherences. Whereas point (i) is used in diffusion measurements already for a long time, points (ii) and (iii) have become increasingly important in high resolution NMR spectroscopy only in recent years replacing or supplementing phase cycling schemes for the selection of a specific coherence transfer pathway (Fig. 1). Eq. (2.30) illustrates the basic principle used. Every application of a PFG introduces a phase factor of the form $\gamma Gz\tau$. For the desired coherence pathway the sum of all these phase factors must be zero. All other pathways do not result in detectable signal if sufficiently strong gradients are used (Eq.2.31). For multiple quantum coherence every operator in the product will evolve according to Eq. (2.30). Consequently the sensitivity of the precession frequency of a coherence to magnetic field gradients, will be proportional to its order. Thus homonuclear double quantum coherence will be two times as sensitive to magnetic field gradients as single quantum coherence, while homonuclear zero quantum coherence will be unaffected. For heteronuclear multiple quantum coherences the different gyromagnetic ratios have to be taken into account (Eq. (2.30)). The application of gradients has the potential to select the desired signal in one scan in contrast to phase cycling which requires the repetition of the experiment and the subtraction of unwanted signals. Unfortunately, only half the signal defocused by a gradient can be refocused if a 90^o *rf* pulse is applied between the two gradients. This drawback can be verified using Eqs. (A.2.6) and (2.30). Such a signal loss constitutes a common feature when gradients are used for pathway selection. As discussed in Section 4.5.3 experimental techniques exist for some cases that prevent this signal loss. Further signal losses can occur due to diffusion losses. In between the defocusing and refocusing gradients the molecules with the nuclei diffuse to a different location preventing a complete refocussing (Eq. 4.3). Diffusion losses are largest for small molecules particularly the solvent magnetization.

Magnetic field gradients can also be applied in the form of spatially inhomogeneous radio-frequency pulses [74, 75]. Either using the inherent *rf* inhomogeneity of the transmitter coil or using a separate coil designed to deliver inhomogeneous B_1 fields [76]. The first method is frequently used in the form of spin-lock purge pulses which destroy magnetization components that are not

aligned along the axis defined by the phase of the *rf* pulse [77]. The second more efficient method requires special hardware and has not yet found many applications. Radio-frequency gradients possess the inherent advantage over static pulsed magnetic field gradients that they can be applied frequency selective [78]. On the other hand limitations arise due to *rf* heating effects and the rather modest maximal strength for *rf* gradients which typically is limited to 0.1T/m.

2.4 Data acquisition

2.4.1 Digitizing the signal

At the end of a pulse sequence the free induction decay (FID) of the magnetization of one nuclear species is measured. The sensitivity of the detection is proportional to $\gamma^{3/2}$ (Eq. (4.2)), and whenever feasible the magnetization should be transferred to and detected on the nuclear species with the largest gyromagnetic ratio. This procedure requires an efficient coupling between the different species of nuclei to retain the sensitivity advantage despite of the inevitable signal losses during the transfer. When working with macromolecules in solution the proton constitutes the preferred nucleus for detection. However, irrespective of the nuclear species detected, the resonance frequency is dozens or hundreds of MHz. Whereas the difference of resonance frequencies of one particular nuclear species in different environments, the chemical shift range, is very small, often only a few kHz. Technically speaking a high frequency, the carrier frequency, is modulated by low frequency signals which represent the spectrum of interest. Subtracting the carrier frequency from the signal one obtains a modified signal that contains only frequencies between zero and a few kHz. Spectrometers use frequency mixing schemes to transform the high resonance frequencies to a lower frequency range since the necessary high dynamic range digitizers exist only up to frequencies of a few hundred kHz. In addition a quadrature detection scheme (Section 3.3.1) delivers two signals which are 90^o out of phase which allows discrimination between positive and negative frequencies with respect to the carrier frequency. The carrier frequency and the frequency of the *rf* pulses on the observe channel are usually identical and consequently quadrature detection enables the user to place the carrier in the middle of the spectrum resulting in a more efficient excitation of the resonances (Fig. 7). The low frequency analog signal thus obtained is digitized at equidistant time points and stored on a computer.

The sampling theorem [79] specifies that for the representation of the analog signal in digital form the sampling rate of the digitizer must be at least twice the highest frequency in the signal. With a quadrature detection system the highest frequency in the spectrum is half the spectral range covered by the signals. In other words, the time increment, the dwell time Δ, between two digitized points must be equal to or smaller than the inverse of the sweep width $2\nu_N$ which covers the frequency range from $-\nu_N$ to $+\nu_N$ with the carrier frequency being at zero frequency. Slower sampling results in folding of the signals with absolute frequencies larger than ν_N into the spectral range of interest. The folded signals will be represented by a wrong frequency and in general will have a phase that differs from the one of unfolded signals. One dimensional ^{1}H NMR spectra of proteins contain a very large number of resonances and folding of additional signals into the spectral range is not desired. This is in contrast to multidimensional experiments where folding quite frequently helps to reduce the spectral range in additional dimensions.

The data can be digitized with two different sampling techniques. The first method digitizes the two quadrature channels simultaneously and delivers data points that can be regarded as complex

numbers. This simultaneous digitization method simply measures the orthogonal components of the precessing magnetization which correspond to the two quadrature channels. The minimal sampling rate $1/\Delta$ becomes equal to the sweep width $2\nu_N$ and a complex Fourier transform of the FID produces the spectrum. The second method digitizes the two quadrature channels sequentially with a sampling rate of $4\nu_N$. Consequently two time shifted signals are measured and correct processing requires that every second data point pair must be inverted in sign before the signal is submitted to a real Fourier transformation resulting in the spectrum [80]. The sequential digitization can be understood using the concept of the rotating frame of reference at the carrier frequency (Fig. A1 in the Appendix). Including the effect of the sign inversion the sampling method corresponds to a sequential sampling of the magnetization components along the *x, y, –x, –y, x, y, –x,* ... axis in the rotating frame. From one digitized point to the next the axis along which the magnetization is sampled rotates by 90^o about the *z* axis instead of being static as with simultaneous digitization. In other words the reference frame for detection rotates within two dwell times by 360^o with respect to the carrier frequency which corresponds to a frequency shift of ν_N. Consequently, the zero frequency shifts from the middle to the edge of the spectrum and all resonance lines have a frequency larger than zero that lies between 0 and $2\nu_N$. This detection scheme is based on a linear phase incrementation with time and is referred to as TPPI method which stands for time-proportional-phase-incrementation [80, 81].

The requirement for a constant dwell time and the sampling theorem are consequences of the Fourier transformation method used to obtain the spectrum from time domain data. Other transformation methods permit varying dwell time lengths. In general, time periods in the FID which have better signal-to-noise ratio (*S/N*) should be sampled more frequently than those with less *S/N*. Different sampling schemes were proposed in combination with maximum entropy reconstruction for the transformation into the frequency domain [82–84]. Considering the modest benefits obtained, these procedures do not seem to be justified in most applications due to the increased complexity involved in the data collection, transformation, and sensitivity to parameter settings. Currently, equidistant sampling is by far the most frequently used scheme.

2.4.2 Handling the water resonance

Many NMR measurements with biological macromolecules rely on the presence of exchangeable protons in the molecules and must therefore be performed in H_2O solutions which contain only a small amount of D_2O for the field-frequency lock (Section 3.3.3). Measuring the spectrum of a protein dissolved in H_2O at a typical concentration of 1 mM requires a dynamic range of the spectrometer which cannot be obtained without the reduction of the signal intensity of the water. Numerous techniques for the reduction of the intense solvent line have been developed and a number of excellent reviews on these techniques exist [*e.g.* 21, 85]. Here only a few selected techniques can be mentioned. When 2D methods were first developed it was a real challenge to obtain spectra from H_2O solutions and initial success was achieved by presaturation of the water resonance [86]. Later spin-lock pulses were introduced which destroy the water magnetization due to the spatial *rf* field inhomogeneity during the pulse [77]. Unlike solvent presaturation which happens during the relaxation delay spin-lock pulses occur later in the sequence allowing the water to recover during the relaxation delay reducing the degree of saturation of the water magnetization. This enhances the signal intensities of exchangeable protons of the protein, for example for the amide protons which play an important role for many experimental schemes. Magnetic field gradients act in a very similar way to spin-lock pulses, however, often better suppression can be obtained [69, 70, 87]. Work at higher pH demands for even better conservation of

water polarization due to the faster exchange rates of labile protons and methods were developed that attempt to conserve the equilibrium water magnetization during the pulse sequence and flip the water back to the positive *z* axis before the start of the acquisition [88].

The huge magnetization of water exhibits special behaviour after the excitation by a *rf* pulse. The magnetization of water rotates back to the positive *z* axis much faster than expected from relaxation. The large signal induced in the receiving coil during precession of the water magnetization creates a magnetic field that acts on the water resonance like a shaped *rf* pulse and rotates it back to the *z* axis. This effect, known as radiation damping, may interfere with the performance of experiments where the water resonance cannot be destroyed, for example when studying interactions between water and protein protons (Section 5.3). When using water flip-back methods [88, 89] the H_2O resonance should never be aligned with the negative *z* axis just prior to acquisition because radiation damping can efficiently rotate the water magnetization into the transverse plane which can overload the receiver system during acquisition. The strength of radiation damping is proportional to the size of the water magnetization and the quality factor of the probe. Consequently it becomes a more serious problem with high magnetic field strengths and higher sensitivity probes. Different techniques have been developed to suppress radiation damping during a pulse sequence without destroying the water resonance. Using pulse field gradients the water can be defocused during periods of free precession and refocused just before the next pulse which is different from 180^o [90]. This procedure conserves the water magnetization except for diffusion losses which must be minimized. Another method temporarily reduces the quality factor Q of the receiving coil and therefore decreases the current induced in the coil and hence the radiation damping effect [91]. This technique requires special circuitry in the probe known as Q switch which allow rapid changes in the Q value. A third method uses an active feed back loop driven by the detected water magnetization. Such a device sends very weak *rf* pulses to the coil counteracting the radiation damping effect. In this way the state of the water magnetization can actively be controlled and suppression as well as an enhancement of the radiation damping effect can be obtained [92, 93].

The very large polarization of water not only interferes with the water resonance itself but slightly alters the main static magnetic field which changes the resonance frequencies of all nuclei. This demagnetizing field effect amounts to a rather small change of the main magnetic field of about 1.5 Hz for protons at 750 MHz when the water magnetization is switched from the positive *z* axis to the negative *z* axis. None the less difference experiments such as hydration experiments may exhibit subtraction artifacts and suffer losses of performance due to these small field changes [94, 95] (Section 5.4).

2.4.3 Decoupling during acquisition

During acquisition of the signal, scalar coupling between nuclei splits the resonance line into different components. Often it would be preferable to decouple the individual nuclei from each other to obtain the best sensitivity and the minimum number of lines. For different species of nuclei decoupling is usually straight forward. For example protons attached to ^{15}N nuclei in labelled proteins can be decoupled from the ^{15}N nuclei by continuous inversion of the magnetization of all the ^{15}N nuclei during acquisition of the proton signal without adverse effects on the measured spectrum. Practical consequences and limitations of heteronuclear decoupling will be discussed in Section 4.3.

Decoupling nuclei of the same species from each other requires more elaborate schemes and, of course, the decoupled nuclei cannot be directly detected. Homonuclear decoupling requires *rf* irradiation at the receiving frequency necessitating that the preamplifier (Section 3.3.1) is switched off during the period of irradiation. The total dwell time, DW_t, is split into a period where the preamplifier is turned off and a period where the signal is received, DW_r. This time sharing reduces the measured signal since the receiver can integrate the signal only during the time DW_r. Switching off the preamplifier reduces not only the signal by a factor DW_r/DW_t but simultaneously the noise proportional to $(DW_r/DW_t)^{1/2}$. For the signal-to-noise $(S/N)_{hd}$ with homonuclear decoupling one obtains the reduction

$$(S/N)_{hd} = (DW_r/DW_t)^{1/2}\ (S/N) \tag{2.32}$$

where *S/N* is the signal-to-noise ratio without decoupling. For example using half the dwell time for homo-decoupling including the necessary switching delays of the hardware reduces $(S/N)_{hd}$ by $\sqrt{2}$ compared to that obtainable without decoupling. Instrumental limitations may reduce the obtainable $(S/N)_{hd}$ further. Not only decoupling but any disturbance which interferes with the integration of the signal reduces the sensitivity, for example, when applying defocusing and refocusing gradients during the acquisition of the signal [96].

2.4.4 Oversampling and digital filtering

Before the signal reaches the digitizer the spectral bandwidth must be limited by a suitable analog filter to the frequency range (sweep width) selected. Otherwise higher frequency noise folds into the spectral region of interest and reduces the obtainable *S/N*. Such analog filters introduce a frequency dependent retardation of the signals and show transient oscillations after a sudden change of the voltage which typically happens at the start of the FID. This characteristic behaviour can result in baseline distortions in the spectrum and the necessity of first order phase correction which itself introduces baseline curvature [97–99]. The distortions in the spectrum due to the filters can be minimized by judicious choice of the time at which the receiver opens and the first data point is sampled [100]. Spectrometers do start accumulation according to this scheme but the appropriate delays usually require fine adjustment for best performance. Use of analog filters present somewhat of a dilemma; on the one hand analog filters introduce distortions which increase with the steepness of the frequency cut off of the filters, on the other hand the filter should be as steep as possible for efficient suppression of signals and noise outside the chosen sweep width. This dilemma can be overcome with oversampling when the digitized frequency range is much larger than the one finally desired. Oversampling allows the use of analog filters with a much broader transition frequency range between full passage and full attenuation. Such filters have short filter delays and negligible transient oscillations which reduces their detrimental effects on the baseline of the acquired spectrum [101]. The analog narrowband filters with steep cutoffs for the adjustment of the final spectral range can then be replaced by digital filters. Special digital signal processors are programmed to apply very steep filters without introducing baseline distortions. The digital signal processors are inserted between the digitizer and the computer memory which stores the data so that the storage requirements of oversampled data does not exceed the space used by conventionally acquired data. Oversampling provides a further advantage by increasing the dynamic range of the digitizer [102]. The extra bits *n* obtained with oversampling can be calculated from the following expression

$$n = \log_2(SW_{ov}/SW) / 2 \tag{2.33}$$

where SW_{ov} is the oversampled frequency range, SW the desired spectral range and the logarithm is base 2. For example, with SW = 10 kHz and SW_{ov} = 160 kHz the effective dynamic range of a 16 bit digitizer corresponds to 18 bits.

The quadrature detection scheme used in spectrometers (Section 3.3.1) requires a phase difference of exactly 90^o and identical amplification in the two signal paths which in practice cannot be achieved. As a consequence positive and negative frequencies with respect to the carrier cannot be completely separated, leaving typically less than 1% of the wrong signal as a quadrature image on the wrong side of the carrier frequency. Still, these signals may have a detrimental effect in multidimensional NMR spectra which contain resonances with widely different signal intensities. The images can usually be suppressed beyond detection by exchanging the signal pathways in subsequent scans which are added [97]. This cancellation method requires simultaneous changing of the phases of all *rf* pulses and the receiver by 90^o between scans. When this procedure is extended to a four-step phase cycle using the phases 0^o, 90^o, 180^o and 270^o it is called CYCLOPS [103]. In addition to the quadrature images CYCLOPS suppresses the spike at zero frequency which is caused by different *dc* offsets in the two receiver channels. When the carrier is set on-resonance with H_2O the original two step phase cycle suffices since the water resonance usually causes a distortion at zero frequency which is much larger than the zero frequency spike. Modern spectrometers use a different scheme sometimes referred to as digital quadrature detection. In this scheme the signal is mixed to a low frequency range which does not contain zero frequency. A narrow bandpass filter programmed into the digital signal processor used to reduce oversampled data then selects the desired spectral range which does not contain quadrature images. The technique produces spectra which cannot contain quadrature images and hence renders CYCLOPS unnecessary which reduces the phase cycling schemes, a definite advantage in multidimensional NMR spectroscopy where phase cycles may be longer than necessary to obtain sufficient signal-to-noise causing unnecessary long experiment times.

2.5 Multidimensional NMR

Multidimensional NMR was first proposed in 1971 [3] and first applications were published a few years later [4]. A multidimensional data set depends on different time variables which can be transformed into multiple frequency domains. For the introduction of an additional time variable a suitable delay during the pulse sequence, the evolution time, is incremented during the experiment [16, 40, 104]. Only during the last time period the signal is physically acquired which is thus often referred to as the direct dimension in contrast to all other dimensions referred to as indirect dimensions. The magnetization measured depends on the evolution times during the pulse sequence and this dependence is reflected by a change in amplitude and/or phase of the acquired signal. A typical *n*-dimensional NMR experiment follows the scheme

$$\text{excitation - (evolution - mixing)}_{n-1} \text{ - detection} \tag{2.34}$$

where the bracket repeats (n–1) times. In a simple example the excitation just consists of a 90^o pulse and the single mixing could be another 90^o pulse which mixes the non-equilibrium states obtained after the first pulse and the evolution time. This sequence is usually referred to as COSY experiment [3, 4]. The sampling of frequencies in evolution periods must fulfil the same requirements with respect to folding and the sampling theorem as the measurement of the FID in the detection period. A subsequent *n*-dimensional Fourier transform provides a *n*-dimensional spec-

trum that depends on *n* frequency variables. If two nuclei suitably interact with each other in a mixing time between two evolution periods or between the last evolution time and the detection period this interaction will be manifested by a resonance in the spectrum, a cross peak, at a position characterized by the precession frequencies of the interacting nuclei. Nuclei that did not have any interaction in the mixing time will show the same frequency in the two successive evolution times. The later resonances, for example, form the diagonal resonances observed in homonuclear 2D spectra. Magnetization components that relax during the scheme will show zero frequency for all evolution periods that occurred before the magnetization relaxed. Such signals are called axial peaks and are usually not of interest.

The number of dimensions measured should be kept minimal since increasing their number reduces the sensitivity due to the additional quadrature sampling step (see below), larger signal losses due to relaxation and additional *rf* pulses. Theoretical considerations show that *n*D spectra do not offer fundamentally new information but are just the mathematical products of the corresponding basic 2D experiments [105]. More than two dimensions should mainly be used to reduce spectral overlap. Most multidimensional experiments are run with two or three dimensions. Only for few experiments a four-dimensional (4D) scheme may be beneficial. One example for a rather frequently used 4D experiment is a homonuclear [^{1}H, ^{1}H]-NOESY which is resolved into a ^{13}C and a ^{15}N dimension [106].

Based on the scheme given in Eq. (2.34) every evolution time is represented by a separate dimension in the spectrum. But experiments can be designed which combine the information from different evolution periods into one dimension. The basic principle of these experiments is very simple. Whenever two evolution times are incremented simultaneously the corresponding frequencies occur in one spectral dimension reducing the number of dimensions by one but keeping the same information [107, 108]. In such experiments one frequency is encoded conventionally on the chemical shift scale. This signal is modulated by the offset frequency of the second nucleus leading to a splitting similar to a *J* coupling but representing the second chemical shift. Hence, the carrier frequency for the second nucleus must be set to one edge of the spectrum since positive and negative frequencies with regard to the carrier result in the same splitting. The chemical shifts of the two nuclei are obtained from the center frequency of the two lines and from their splitting [107, 108].

In multidimensional spectra, resonances should have absorptive lineshapes in all dimensions for the best spectral resolution and quality of a *n*D spectrum. To prevent the undesirable mixture of absorptive and dispersive signals the two orthogonal transverse magnetization components represented by the operators I_x and I_y must be obtained separately from the final signal. In the framework of coherence pathways both $+k$ and $-k$ coherence levels of a k quantum coherence during an evolution time must be maintained [16, 40] which then allows to separate the operators I_x and I_y in the final signal. For practical applications this requires that sine and cosine components of the signal during the evolution time are not mixed when accumulating the data. In other words these components should not be summed into one FID otherwise only *n*- or *p*-type peaks are obtained which do not have a pure phase; *p*-type peaks result from a coherence pathway whose coherence levels have the same sign during the evolution and final detection period, opposite signs lead to *n*-type peaks [16] (Fig. 1).

In analogy to the direct acquisition of the signal a quadrature scheme must be applied in the indirect dimension. For the indirect dimensions the sine and cosine components of the signal cannot be measured simultaneously. The two quadrature components are typically sampled consecu-

tively changing the phase of the 90° *rf* pulse at the start of the evolution time by 90° according to one of the schemes given in Table 3. This procedure reduces the sensitivity for every additional dimension by a factor $\sqrt{2}$. With respect to sensitivity it is important to note that all noise in the spectrum originates from the measurement in the direct dimension. During the evolution periods the signal may be reduced due to relaxation but no noise is added. As there is no noise to be excluded from the bandwidth of interest there is no need for filters in the indirect dimensions. None the less the baseline in indirect dimensions may be distorted. This baseline distortion originates from linear phase corrections applied in the indirect dimensions. Therefore linear phase corrections must be avoided by adjusting the initial delay of the evolution time properly. In principle the minimal evolution time should be zero. Often this delay cannot be zero. For example, the finite duration of the *rf* pulses at the beginning and at the end of the evolution period result in evolution of the magnetization requiring a linear phase correction for an absorptive spectrum. It is customary to sample the first point at half the dwell time. For data sampled as complex data points this requires a linear phase correction of 180° across the spectrum which does not introduce baseline curvature [97, 99]. As an additional advantage folded peaks have opposite sign and are easily detected if they do not overlap with an unfolded resonance line. This feature proves useful in some instances to reduce the spectral range together with the number of increments required, as for example in the indirect carbon dimension of heteronuclear multidimensional spectra [109]. Hence folding can be used to extend the phase cycling and/or to reduce disk storage requirements.

For quadrature detection in indirect dimensions several techniques are available [110] (Table 3). The individual schemes sample the data at different time points and with a different sign which requires suitable Fourier transform (FT) algorithms to be used. The particular method affects both the frequency position of the axial peaks and the folding behaviour for resonances outside

Table 3
Properties of different quadrature sampling schemes

quadrature scheme	sampling of x and y components‡ n	n+1	n+2	n+3	FT mode	axial peaks[f]	folded peaks[†]
Redfield	x(t)	y(t+Δ/2)	x(t+Δ)	y(t+3Δ/2)	real[§]	center	mirrored
TPPI	x(t)	y(t+Δ/2)	–x(t+Δ)	–y(t+3Δ/2)	real	edge	mirrored
Complex	x(t)	y(t)	x(t+Δ)	y(t+Δ)	complex	center	cyclic
Complex-TPPI	x(t)	y(t)	–x(t+Δ)	–y(t+Δ)	complex[§]	edge	cyclic

‡ The four columns indicate consecutive time points at which four magnetization components are sampled which evolve during the evolution time, the time period Δ stands for the dwell time which is equal to the inverse of the frequency range sampled; x(t) and y(t) refer to the x- and y-component at time point t, respectively; the sign indicates the use of the positive or negative component.

[f] Axial peaks appear either in the center or at the edge of the spectral range selected.

[†] Folded peaks are either mirrored at the closer edge of the spectral range or cyclically shifted into the spectrum by subtraction of the spectral range.

[§] Every second pair of data points in the indirect dimension has to be inverted in sign before Fourier transformation (FT), the same goal can be achieved by changing the phase setting of the receiver by 180°.

the selected spectral range (Table 3). The best overall performance can be expected using a combination of complex sampling [111] with TPPI phase incrementation [81]. This scheme allows to adjust the initial delay to obtain optimal baseline behaviour and at the same time places axial peaks at the edge of the spectrum [110]. In principle, axial peaks are suppressed using a suitable phase cycling scheme, for example the phase cycle x, –x applied to the excitation pulse and the receiver. None the less residual intensity should still be moved to the edge of the spectrum. TPPI [81] and Redfield [80] quadrature detection are nowadays only used when their specific folding properties are required.

2.6 Data processing

2.6.1 Transforming the time domain data into a spectrum

A detailed description of data processing methods used in biomolecular NMR is outside the scope of this article. There are excellent monographs dealing with all aspects of data processing in detail [112–114]. Here only a few basic aspects shall be mentioned. In NMR time dependent oscillations of the magnetization are measured which can be represented in an analytical form as a complex signal $S(t)$.

$$S(t) = \sum_k \exp(2i\pi\nu_k t) \exp(-t/T_{2k}) \tag{2.35}$$

where ν_k are the individual resonance frequencies and T_{2k} the corresponding transverse relaxation times. The frequency components ν_k encoded in the modulation are typically analysed by a complex Fourier transformation resulting in a spectrum with a real part containing absorptive lines $A_k(\nu_k-\nu)$ of the form

$$A_k(\nu_k-\nu) = T_{2k}/(1+4\pi^2 T_{2k}^2(\nu_k-\nu)^2)) \tag{2.36}$$

and an imaginary part containing dispersive lines $D_k(\nu_k-\nu)$

$$D_k(\nu_k-\nu) = 2\pi T_{2k}^2(\nu_k-\nu)/(1+4\pi^2 T_{2k}^2(\nu_k-\nu)^2)) \tag{2.37}$$

In practice the signals in the real part of the spectrum may not be completely absorptive due to a phase factor in the modulation of the signal. By a suitable mixing of the real and imaginary parts using a phase correction routine, absorptive lines can be obtained in the real part and dispersive lines in the imaginary part of the spectrum. Absorptive lineshapes are preferred since they have narrower lineshapes (Eq. (2.36) and (2.37)) and hence offer a better resolved spectrum. In multidimensional NMR experiments, proper acquisition schemes have to be used to avoid summation of absorptive and dispersive lines in the real part of the spectrum (Table 3). A sum of absorptive and dispersive resonances cannot be corrected by a mathematical procedure and severely degrades the spectral quality. Alternative analysis methods to Fourier transformation are available but are not frequently used because they often require extensive calculation times, are nonlinear algorithms which may distort the signal intensities and the quality of the results is sensitive to parameter settings [113, 114].

Because the causality principle requires the measured FID to be zero for times smaller than zero Fourier transformation of the FID leads to a relation (Kramers-Kronig relation) between the real

and imaginary part of the spectrum [16]. The two parts can be calculated from each other by a Hilbert transformation. Since Fourier transformation results in a real and an imaginary part with identical information content the number of data points *N* in the FID must be doubled by adding *N* zeroes at the end of the FID (zero filling). In this way *N* independent data points in the FID are represented by *N* independent data points in the spectrum. More zero filling does smooth the representation of the data by interpolation but no additional information can be obtained [7, 115]. To avoid truncation artifacts which result in oscillations around individual signals zerofilled FIDs must be brought smoothly to zero by multiplication with a weighting function which becomes zero at the end of the FID.

The first data point in the FID is often measured as close as possible to the time point zero in order to avoid a first order phase correction in the spectrum. With this procedure the intensity of the first time domain data point should be averaged with the last data point in the FID to result in a properly periodic signal [116], in practice this is often equivalent to a division of the first point by two. The first data point represents the integral of the spectrum and overemphasizing its intensity adds a constant offset to the spectrum which can be very disturbing in multidimensional spectra since the offset usually varies from trace to trace. NMR software provides the possibility to scale the first point to remove the baseline offset. In indirect dimensions where the measurement starts after half a dwell time the situation is different. In this case the first data point represents the correct integral and no additional scaling is necessary but a linear phase correction of 180^o has to applied across the spectrum.

In multidimensional experiments the maximal evolution time in indirect dimensions must often be chosen to be rather short to achieve the best sensitivity and therefore often truncated FIDs are obtained for indirect dimensions. Applying weighting functions directly to truncated FIDs discards some of the measured signal. In this situation linear prediction provides a possibility to extend the experimental data in the time domain before applying weighting functions [113]. However, typically used algorithms determine four parameters for every signal: frequency, intensity, linewidth, and phase. Enough data points must be available to prevent overfitting the data and the number of predicted points should as a rule of thumb not exceed the number of measured points. Linear prediction works best when the time-domain data to be extended contains a small number of signals. In order to achieve this, all of the other dimensions of the spectrum should be Fourier transformed before linear prediction in a given dimension. If more than one dimension is to be linear predicted inverse Fourier transformations will be necessary. It should be noted that in the first round of Fourier transformations window functions are not applied because this would throw away information present in the FID. Even with linear prediction the resulting spectrum in an indirect dimension of a 3D and especially a 4D experiment may still have a resolution of only 40 Hz/point or even less. Applying resolution enhancement filters to FIDs with such a low resolution is of little use and often simple cosine functions are applied. There are a variety of commercial and non commercial programs which allow interactive evaluation of NMR data using a graphics interface. However for time consuming calculations, such as linear prediction or sophisticated baseline correction algorithms, it may be advantageous to use a program with no graphic interface to enable processing in batch mode on high performance computers [117, 118].

2.6.2 Referencing the chemical shift

The nuclear shielding constant σ_i describes the effect of magnetic interactions between electrons and nuclei which affect the local magnetic field B_i experienced by the nucleus i with $B_i = (1–\sigma_i)B_o$, and hence influences its resonance frequency. This chemical shift has long been known to be extremely sensitive to a multitude of structural, electronic, magnetic and dynamical variables and in principle contains a wealth of information on the state of the system under investigation. This potential is largely offset by the difficulties of a detailed interpretation which attributes the measured chemical shift to the various contributions. However, the large amount of data represented by the ^{1}H, ^{13}C and ^{15}N shifts in known 3D NMR structures of proteins forms the basis for a multitude of empirical and semi-empirical correlations with structural parameters. These correlations can be used during the assignment process as an additional source of information [15, 119–122]. It is also possible to refine protein structures based on chemical shifts and even with insufficient information for a structure determination chemical shifts can be used to distinguish between alpha helix and beta sheet *via* the chemical shift index [120, 123]. This index provides a simple tool for identifying protein secondary structure through analysis of backbone ^{13}C chemical shifts. Further information on many aspects of the use of chemical shifts in studies of proteins can be found in a recent review article [124].

The evaluation of chemical shift data requires an accurate referencing of NMR spectra both for reproducibility and for the correlation of the chemical shift with structural properties. A wide variety of reference compounds exist for various solvents and many nuclei. Referencing each nuclear species individually is cumbersome and prone to errors. Reference substances may interact with the protein or not be soluble in water. In addition the reference chemical shift may depend on parameters like temperature, pH or ionic strength. External referencing circumvents most of these problems. However, separating the solution and the standard into two compartments introduces susceptibility effects which depend on the sample geometry and disappear only for spherical inserts. With the proton omnipresent in biological samples indirect referencing of the heteronuclei to a proton standard becomes attractive. Recently it was proposed to exclusively use dimethylsilapentane sulfonic acid (DSS) as standard for referencing of proton chemical shifts due to its favourable properties as a reference compound and to relate standards for heteronuclei to DSS by a scaling factor Ξ which is specific for a selected heteronuclear standard [125]. The absolute methyl proton frequency in DSS in the sample at a given field is simply multiplied by Ξ to obtain the zero frequency for the heteronuclear chemical shift scale. Values of Ξ for ^{13}C and ^{15}N [125] as well as for ^{19}F and ^{31}P [126] have been published for the standards 10mM DSS in water (DSS), liquid NH_3 (NH_3), trifluoroacetic acid (TFA), and 85% ortho-phosphoric acid (H_3PO_4), respectively, and are reproduced in Eqs. [2.38]–[2.42]

$$\Xi\ (^1\text{H, DSS}) = 1.000000000 \tag{2.38}$$
$$\Xi\ (^{13}\text{C, DSS}) = 0.251449530 \tag{2.39}$$
$$\Xi\ (^{15}\text{N, } NH_3) = 0.101329118 \tag{2.40}$$
$$\Xi\ (^{19}\text{F, TFA}) = 0.940866982 \tag{2.41}$$
$$\Xi\ (^{31}\text{P, } H_3PO_4) = 0.404807356 \tag{2.42}$$

In practice the frequency difference between the methyl proton resonance of DSS and the carrier (usually at the water resonance) must be subtracted from the absolute frequency of the carrier to obtain the zero ppm reference for protons. Chemical shifts referenced to a variety of different reference compounds can be readjusted to conform to the indirect referencing discussed above using published conversion data [125].

The low digital resolution typically obtained in 3D and 4D NMR spectra makes calibration critically dependent on the spectral data point that represents the position of the carrier frequency. In general the number of points *N* contained in a NMR spectrum is a power of 2. Assuming a numbering of the points from 1 to N the question arises if the carrier frequency is represented by point $N/2 - 0.5$ or by point $N/2 + 0.5$. Using the fact that the frequency domain spectrum is a periodic function point 1 and point N + 1 have identical values and hence point N + 0.5 represents the position of the carrier frequency. However, the implementation in the software used may be different. When details of the transformation software are not known, a simple test allows determination of the position of the carrier frequency in the spectrum. Adding a constant to the FID before Fourier transformation will create a spike in the spectrum which appears at the carrier frequency.